

IQ Skew and Imbalance Estimation for Coherent Point-to-Multi-Point Optical Networks

Ji Zhou, Jianrui Zeng, Haide Wang, Dong Guo, Liangchuan Li, Weiping Liu, and Changyuan Yu

Abstract—Coherent point-to-multi-point (PtMP) optical network based on digital subcarrier multiplexing (DSCM) has been a promising technology for metro and access networks to achieve cost savings, low latency, and high flexibility. In-phase and quadrature (IQ) impairments of the coherent transceiver (e.g. IQ skew and power imbalance) cause severe performance degradation. In the DSCM-based coherent PtMP optical networks, it is hard to realize far-end IQ-impairments estimation for the hub transmitter because the leaf on one subcarrier cannot acquire the signal on the symmetrical subcarrier. In this paper, we propose a far-end IQ-impairments estimation based on the specially designed time-and-frequency interleaving tones (TFITs), which can simultaneously estimate IQ skews and power imbalances of the hub transmitter and leaf receiver at an individual leaf. The feasibility of the TFITs-based IQ-impairments estimation has been experimentally verified by setting up 8Gbaud/SC \times 4SCs DSCM-based coherent PtMP optical network. The experimental results depict that the absolute errors in the estimated IQ skew and power imbalance are within $\pm 0.5\text{ps}$ and $\pm 0.2\text{dB}$, respectively. In conclusion, TFITs-based IQ-impairments estimation has great potential for DSCM-based coherent PtMP optical networks.

Index Terms—Coherent PtMP optical networks, DSCM, IQ-impairments estimation, IQ skew, and power imbalance.

I. INTRODUCTION

DRIVEN by emerging network services, hub and spoke (H&S) networks have become the main network architecture for access and metro networks [1]–[3]. Coherent point-to-multi-point (PtMP) optical networks enabled by digital subcarrier multiplexing (DSCM) are the optimal solutions for matching the requirements of H&S networks [4]–[6]. Compared to coherent point-to-point (P2P) optical networks, the DSCM-based coherent PtMP optical networks can provide massive connections between a high-speed hub node and multiple low-speed leaf nodes, achieving cost savings, lower latency, and higher flexibility [7]–[9]. However, in-phase and quadrature (IQ) impairments of the coherent transceiver (e.g.

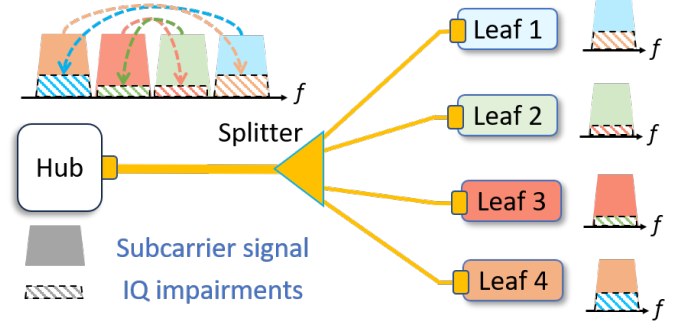


Fig. 1. Schematic diagram of DSCM-based coherent PtMP optical networks with Tx IQ impairments.

IQ skew and power imbalance) cause image crosstalk between the symmetrical subcarriers of the DSCM signal. Particularly, the image crosstalk caused by IQ skew grows with the increase of the subcarrier frequency [10]–[12]. Therefore, the image crosstalk causes significant performance degradation on the leaves carried by the high-frequency subcarriers [13]–[15].

The IQ impairments of the coherent transceiver have been widely studied for coherent P2P optical networks. The transmitter (Tx) IQ impairments can be extracted from the tap coefficients of the multiple-input multiple-output (MIMO) equalizer, which has been widely applied in the single-carrier coherent P2P optical networks [16]–[18]. Furthermore, the 4×4 MIMO equalizer has been recently proposed to estimate Tx IQ impairments for DSCM-based coherent P2P optical networks by processing symmetrical subcarrier pairs [19], [20]. In addition, Tx IQ-impairments estimation based on a specially designed training sequence is proposed for coherent P2P optical networks. The uniformly-spaced frequency tones are used to acquire the Tx IQ skew by calculating the slope of their phase difference [21], [22]. Another method based on the single sideband comb signals is proposed to estimate the Tx IQ impairments by analyzing the image spectrum [23].

Figure 1 shows the schematic diagram of coherent PtMP optical networks based on DSCM with Tx IQ impairments. The hub transmits the DSCM signal with four subcarriers to the leaves, and one leaf receives its corresponding subcarrier rather than symmetrical subcarrier pairs. The above-mentioned schemes for coherent P2P optical networks require the whole spectrum of the transmitted signal to estimate the Tx IQ impairments, which are difficult to apply in DSCM-based coherent PtMP optical networks. This paper proposes the first far-end IQ-impairments estimation for the DSCM-based coherent PtMP optical networks, which can accurately

Manuscript received; revised. This work was supported in part by the National Key R&D Program of China under Grant 2023YFB2905700, in part by the National Natural Science Foundation of China under Grant 62371207 and Grant 62005102, and in part by the Young Elite Scientists Sponsorship Program by CAST under Grant YESS20230194. (Corresponding author: Dong Guo and Liangchuan Li.)

Ji Zhou, Jianrui Zeng, Haide Wang, and Weiping Liu are with Department of Electronic Engineering, College of Information Science and Technology, Jinan University, Guangzhou 510632, China.

Dong Guo is with School of Information and Electronics, Beijing Institute of Technology, Beijing 100081, China.

Liangchuan Li are with Optical Research Department, Huawei Technologies Co Ltd, Dongguan, 523808, China.

Changyuan Yu is with Department of Electronic and Information Engineering, The Hong Kong Polytechnic University, Hong Kong.

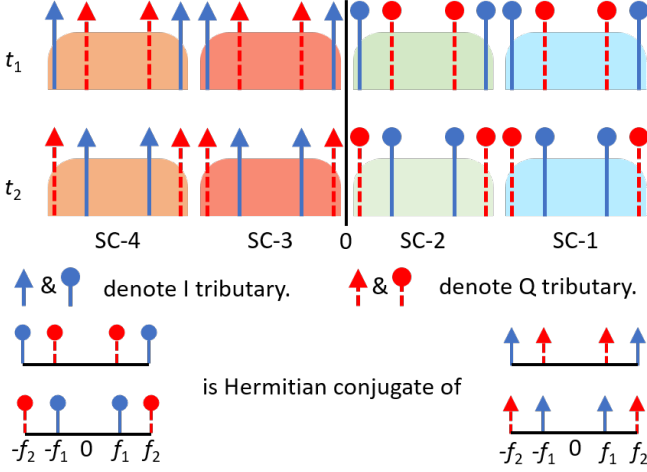


Fig. 2. Structure of the specially designed TFITs for one polarization.

estimate IQ skews and power imbalances of the hub Tx and leaf receiver (Rx) at the leaf. The main contributions of the work are as follows:

- Time-and-frequency interleaving tones (TFITs) are specially designed to accurately estimate the IQ impairments for the DSCM-based coherent PtMP optical networks, which solves the challenge of the far-end IQ-impairments estimation at an individual leaf.
- 8Gbaud/SC \times 4SCs DSCM-based coherent PtMP optical network is experimentally demonstrated to verify the feasibility of the TFITs-based IQ-impairments estimation. The absolute errors in the estimated IQ skew and power imbalance are within $\pm 0.5\text{ps}$ and $\pm 0.2\text{dB}$, respectively.

The remainder of the paper is organized as follows. In Section II, the TFITs structure is designed to estimate IQ impairments. For DSCM-based coherent PtMP optical networks, the principle of IQ-impairments estimation is introduced. In Section III, we introduce the experimental setups of a DSCM-based coherent PtMP optical network. In Section IV, the experimental results and discussions are demonstrated to verify the performance of the TFITs-based IQ-impairments estimation. Finally, the paper is concluded in Section V.

II. TFITs STRUCTURE AND ESTIMATION PRINCIPLE

In this section, the TFITs structure for IQ-impairments estimation is designed for the DSCM-based coherent PtMP optical networks. Then the TFITs affected by IQ impairments are analyzed. Finally, the principle of TFITs-based far-end IQ-impairments estimation is given.

A. TFITs Design for IQ-impairments estimation

The specially designed TFITs structure for one polarization is shown in Fig. 2. The first subcarrier (SC-1) and fourth subcarrier (SC-4) are a pair of symmetrical subcarriers, while the second subcarrier (SC-2) and the third subcarrier (SC-3) are a pair of symmetrical subcarriers. Taking the symmetrical SC-1 and SC-4 into consideration, after the frequency shift,

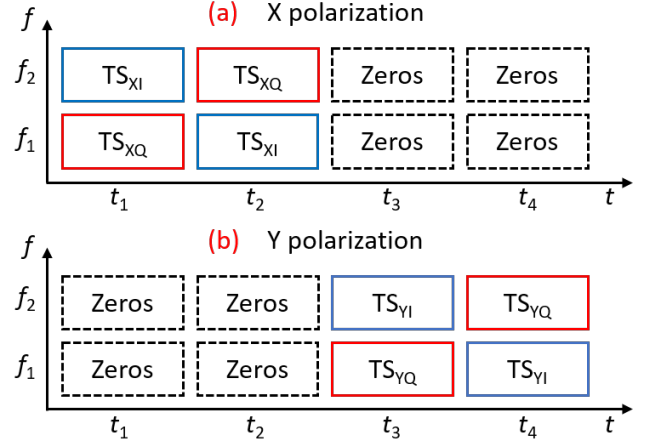


Fig. 3. The specially designed TFITs including four time slots t_1, t_2, t_3, t_4 and two tone frequencies f_1, f_2 for (a) X polarization and (b) Y polarization.

the intermediate frequency signal $s_1(t)$ of SC-1 and $s_4(t)$ of SC-4 can be expressed as

$$s_1(t) = [I_1(t) + jQ_1(t)]e^{+j2\pi f_c t} \quad (1)$$

and

$$s_4(t) = [I_4(t) + jQ_4(t)]e^{-j2\pi f_c t}, \quad (2)$$

respectively. The center frequencies of the SC-1 and SC-4 are $+f_c$ and $-f_c$, respectively. $I_1(t) + jQ_1(t)$ and $I_4(t) + jQ_4(t)$ are the baseband signal on the SC-1 and SC-4, respectively. Therefore, the training sequence (TS) $s_{\text{Tx}}(t)$ is generated as

$$s_{\text{Tx}}(t) = s_1(t) + s_4(t) = s_{\text{Tx},I}(t) + js_{\text{Tx},Q}(t) \quad (3)$$

where $s_{\text{Tx},I}(t)$ and $s_{\text{Tx},Q}(t)$ are the I and Q tributaries of the TS $s_{\text{Tx}}(t)$, which can be expressed as

$$s_{\text{Tx},I}(t) = [I_1(t) + I_4(t)] \cos 2\pi f_c t + [Q_4(t) - Q_1(t)] \sin 2\pi f_c t \quad (4)$$

and

$$s_{\text{Tx},Q}(t) = [I_1(t) - I_4(t)] \sin 2\pi f_c t + [Q_1(t) + Q_4(t)] \cos 2\pi f_c t, \quad (5)$$

respectively. As Fig. 2 shows, each subcarrier consists of two tones at the frequencies f_1 and f_2 , which can be defined as $I_{f_1}(t) + jQ_{f_1}(t)$ and $I_{f_2}(t) + jQ_{f_2}(t)$, respectively. In the time slot t_1 , the tone at the frequency f_1 inserted on SC-4 is the Hermitian conjugate of that inserted on SC-1. In other word, $I_1(t) + jQ_1(t)$ is equal to $-I_4(t) + jQ_4(t)$ where $I_1(t)$ and $Q_1(t)$ are equal to $I_{f_1}(t)$ and $Q_{f_1}(t)$, respectively. Therefore, the Q tributary of TFITs with the frequency $f_1 + f_c$ tone can be expressed as

$$s_{\text{Tx},Q}(t) = 2 \times [I_{f_1}(t) \sin 2\pi f_c t + Q_{f_1}(t) \cos 2\pi f_c t]. \quad (6)$$

The I tributary of the TFITs with the frequency $f_1 + f_c$ tone is zero. Furthermore, the tone at frequency f_2 inserted on SC-4 is the Hermitian conjugate of that inserted on SC-1. In other word, $I_1(t) + jQ_1(t)$ is equal to $I_4(t) - jQ_4(t)$ where $I_1(t)$ and $Q_1(t)$ are equal to $I_{f_2}(t)$ and $Q_{f_2}(t)$, respectively. Therefore,

$$\begin{aligned}
s_{\text{Rx},f_s/2}(t) &= 2 [I_{f_s/2}(t) \cos 2\pi f_c t - Q_{f_s/2}(t) \sin 2\pi f_c t] \times e^{-j[2\pi(f_c + \Delta f)t + \phi]} \\
&= \underbrace{[I_{f_s/2}(t) \quad -Q_{f_s/2}(t)]}_{r_{f_s/2,I}(t)} \begin{bmatrix} \cos \phi_1(t) \\ \sin \phi_1(t) \end{bmatrix} + j \underbrace{[I_{f_s/2}(t) \quad Q_{f_s/2}(t)]}_{r_{f_s/2,Q}(t)} \begin{bmatrix} \sin \phi_1(t) \\ \cos \phi_1(t) \end{bmatrix}
\end{aligned} \quad (13)$$

$$\begin{aligned}
js_{\text{Rx},f_s/4}(t) &= 2jg_{\text{Tx}} [I_{f_s/4}(t + \tau_{\text{Tx}}) \sin 2\pi f_c(t + \tau_{\text{Tx}}) + Q_{f_s/4}(t + \tau_{\text{Tx}}) \cos 2\pi f_c(t + \tau_{\text{Tx}})] e^{-j[2\pi(f_c + \Delta f)t + \phi]} \\
&= g_{\text{Tx}} \underbrace{[I_{f_s/4}(t + \tau_{\text{Tx}}) \quad -Q_{f_s/4}(t + \tau_{\text{Tx}})]}_{r_{f_s/4,I}(t)} \begin{bmatrix} \cos \phi_2(t) \\ \sin \phi_2(t) \end{bmatrix} + jg_{\text{Tx}} \underbrace{[I_{f_s/4}(t + \tau_{\text{Tx}}) \quad Q_{f_s/4}(t + \tau_{\text{Tx}})]}_{r_{f_s/4,Q}(t)} \begin{bmatrix} \sin \phi_2(t) \\ \cos \phi_2(t) \end{bmatrix}
\end{aligned} \quad (14)$$

the I tributary of TFITs with the frequency $f_2 + f_c$ tone can be expressed as

$$s_{\text{Tx},I}(t) = 2 \times [I_{f_2}(t) \cos 2\pi f_c t - Q_{f_2}(t) \sin 2\pi f_c t]. \quad (7)$$

The Q tributary of the TFITs at frequency $f_2 + f_c$ is zero.

Specifically, f_1 and f_2 can be set to be a quarter of the baud rate $f_s/4$ and half of the baud rate $f_s/2$, respectively where $f_s/4$ denotes the baud rate. Therefore, by combining the Eq. (6) and Eq. (7), the TFITs in the time slot t_1 can be expressed as

$$s_{\text{Tx},t_1}(t) = s_{\text{Tx},I}(t) + js_{\text{Tx},Q}(t) = s_{\text{Tx},f_s/2}(t) + js_{\text{Tx},f_s/4}(t). \quad (8)$$

To eliminate the influence on IQ-impairments estimation caused by the phase-frequency response caused by the devices and chromatic dispersion, TFITs are also designed using two time slots with two interleaving frequencies. Compared to time slot t_1 , the frequencies of the I and Q tributaries are interchanged in the time slot t_2 . Therefore, the TFITs in the time slot t_2 can be expressed as

$$s_{\text{Tx},t_2}(t) = s_{\text{Tx},I}(t) + js_{\text{Tx},Q}(t) = s_{\text{Tx},f_s/4}(t) + js_{\text{Tx},f_s/2}(t). \quad (9)$$

The TFITs can be generated by combining the signals of Eq. (8) and Eq. (9). Fig. 3 shows the specially designed TFITs include four time slots $[t_1, t_2, t_3, t_4]$ and two tones at frequencies $[f_1, f_2]$ for (a) X and (b) Y polarizations. At the t_1 and t_2 time slots, the TFITs are carried on the X polarization, while the Y polarization is zero to avoid inter-polarization crosstalk between X and Y polarizations [24]–[26]. At the t_3 and t_4 time slots, the proposed TFITs are carried on the Y polarization, while the X polarization is zero.

B. The Model of IQ Impairments on TFITs

Without loss of generality, we investigate the model of IQ impairment on the TFITs in the time slot t_1 . The TFITs with Tx IQ impairments can be modeled as [27]

$$s_{\text{Tx}}(t) = s_{\text{Tx},f_s/2}(t) + js_{\text{Tx},f_s/4}(t + \tau_{\text{Tx}}) \quad (10)$$

where τ_{Tx} and g_{Tx}^2 represent the Tx IQ skew and power imbalance, respectively. After optical modulation, the launch optical signal can be defined as

$$s_{\text{Tx},O}(t) = [s_{\text{Tx},f_s/2}(t) + js'_{\text{Tx},f_s/4}(t)] e^{j2\pi f_0 t} \quad (11)$$

where f_0 is the center frequency of the optical carrier. $s'_{\text{Tx},f_s/4}(t)$ is defined as $g_{\text{Tx}} s_{\text{Tx},f_s/4}(t + \tau_{\text{Tx}})$.

At the Rx side, SC-1 or SC-4 can be selected by tuning the wavelength of the local oscillator (LO) laser to the frequencies of $f_0 + f_c$ or $f_0 - f_c$, respectively. For SC-1, $s_{\text{Tx},O}(t)$ is multiplied by $e^{-j[2\pi(f_0 + f_c + \Delta f)t + \phi]}$ mathematically, where Δf and ϕ are the frequency offset and phase noise of the laser, respectively. After frequency downshift, the received signal of SC-1 is expressed as

$$\begin{aligned}
s_{\text{Rx}}(t) &= [s_{\text{Tx},f_s/2}(t) + js'_{\text{Tx},f_s/4}(t)] e^{-j[2\pi(f_c + \Delta f)t + \phi]} \\
&= s_{\text{Rx},f_s/2}(t) + js_{\text{Rx},f_s/4}(t)
\end{aligned} \quad (12)$$

where $s_{\text{Rx},f_s/2}(t)$ and $js_{\text{Rx},f_s/4}(t)$ are denoted as Eq. (13) and Eq. (14) show at the top of this page, respectively. $\phi_1(t)$ is $-(2\pi\Delta f t + \phi)$ and $\phi_2(t)$ is $-(2\pi\Delta f t + \phi - 2\pi f_c \tau_{\text{Tx}})$. After frequency downshift, both the I and Q tributaries of the received signal $s_{\text{Rx}}(t)$ contain the $f_s/4$ and $f_s/2$ tones, which can be expressed as

$$s_{\text{Rx}}(t) = r_{f_s/2,I}(t) + r_{f_s/4,I}(t) + j[r_{f_s/2,Q}(t) + r_{f_s/4,Q}(t)] \quad (15)$$

where $r_{f_s/2,I}(t)$, $r_{f_s/4,I}(t)$, $r_{f_s/2,Q}(t)$ and $r_{f_s/4,Q}(t)$ are denoted as Eq. (13) and Eq. (14) shown. Therefore, the I and Q tributaries of the signal $s_{\text{Rx}}(t)$ can be expressed as

$$s_{\text{Rx},I}(t) = r_{f_s/2,I}(t) + r_{f_s/4,I}(t) \quad (16)$$

and

$$s_{\text{Rx},Q}(t) = r_{f_s/2,Q}(t) + r_{f_s/4,Q}(t), \quad (17)$$

respectively. When the received signal suffers the Rx IQ impairments, it can be modeled as [28], [29]

$$s_{\text{Rx}}(t) = s_{\text{Rx},I}(t) + js_{\text{Rx},Q}(t + \tau_{\text{Rx}}) \quad (18)$$

where τ_{Rx} and g_{Rx}^2 denote the Rx IQ skew and power imbalance, respectively.

C. Estimation of Rx IQ Impairments in PtMP Networks

According to the adding order of Tx and Rx IQ impairments, the Rx IQ impairments should be estimated and compensated before estimation for the Tx IQ impairments. Based on the model of Rx IQ impairments, we propose TFITs-based schemes for accurately estimating the Rx IQ skew and power imbalance.

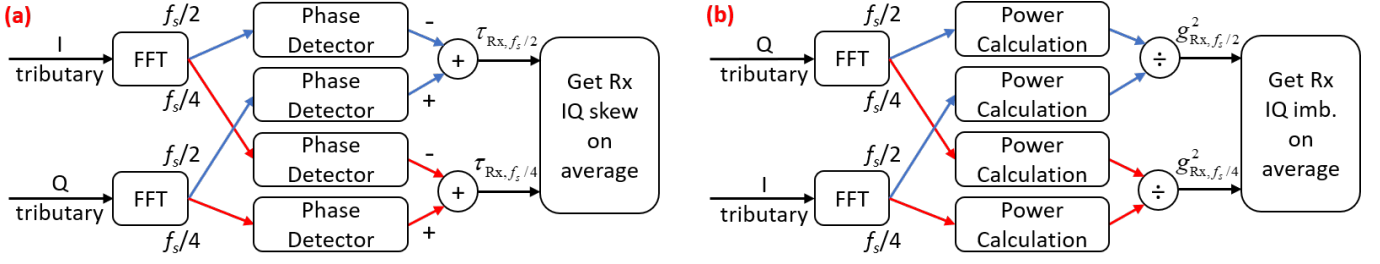


Fig. 4. Schematic diagram of IQ-impairments estimation based on the specially designed TFITs including Rx IQ (a) skew and (b) power imbalance.

1) *Estimation of Rx IQ Skew*: By substituting Eq. (13) and Eq. (14) into Eq. (18), it is inferred that in the time slot t_1 , $r_{f_s/2,1}(t)$ contains only the timing phase offset caused by the out-of-synchronization clock, while $g_{Rx}r_{f_s/2,Q}(t + \tau_{Rx})$ contains both the timing phase offset of the clocks and Rx IQ skew τ_{Rx} . Similarly, there is a difference of Rx IQ skew τ_{Rx} between the timing phase offsets of $r_{f_s/4,1}(t)$ and $g_{Rx}r_{f_s/4,Q}(t + \tau_{Rx})$. Therefore, the Rx IQ skew can be estimated by calculating the difference in the timing phase offset between the Q and the I tributaries of the tones with the same frequency. The natural high signal-to-noise ratio (SNR) of the frequency tones results in a high estimation accuracy.

Figure 4(a) shows the schematic diagram of Rx IQ-skew estimation by using the I and Q tributaries of the Rx TFITs. By performing sampling and fast Fourier transform (FFT) on the I tributary of the received signal $s_{Rx,I}(t)$ to $S_{Rx,I}(k)$ and Q tributary $g_{Rx}s_{Rx,Q}(t + \tau_{Rx})$ to $S_{Rx,Q}(k)$ at each time slot, the timing phase offsets of I and Q tributaries can be calculated by the Godard phase detector using the $2n$ frequency points around $f_s/2$ [30]. Therefore, the Rx IQ skew is estimated by calculating the difference between timing phase offsets of the Q and I tributaries of $f_s/2$ tone, which can be expressed as

$$\tau_{Rx, f_s/2} = \frac{1}{2\pi} \arg \left[\sum_{k=N/4-n+1}^{N/4+n} S_{Rx,Q}(k) S_{Rx,Q}^* \left(k + \frac{N}{2} \right) \right] - \frac{1}{2\pi} \arg \left[\sum_{k=N/4-n+1}^{N/4+n} S_{Rx,I}(k) S_{Rx,I}^* \left(k + \frac{N}{2} \right) \right] \quad (19)$$

where $\arg(\cdot)$ denotes phase extraction and $(\cdot)^*$ denotes conjugate operation. The FFT points of $S_{Rx,I}(k)$ and $S_{Rx,Q}(k)$ around the $N/4$ correspond to the frequency points around $f_s/2$. The timing phase offset can be also calculated by the modified Godard phase detector using the frequency points around $f_s/4$ [31]. Therefore, the Rx IQ skew can be estimated by calculating the difference between timing phase offsets of the Q and I tributaries of $f_s/4$ tone, which is expressed as

$$\tau_{Rx, f_s/4} = \frac{1}{\pi} \arg \left[\sum_{k=3N/8-n+1}^{3N/8+n} S_{Rx,Q}(k) S_{Rx,Q}^* \left(k + \frac{N}{4} \right) \right] - \frac{1}{\pi} \arg \left[\sum_{k=3N/8-n+1}^{3N/8+n} S_{Rx,I}(k) S_{Rx,I}^* \left(k + \frac{N}{4} \right) \right] \quad (20)$$

where the FFT points of $S_{Rx,I}(k)$ and $S_{Rx,Q}(k)$ around the $3N/8$ correspond to the frequency points around $f_s/4$. Finally, the more accurate Rx IQ skew $\tau_{Rx,IQ}$ can be obtained by averaging $\tau_{Rx, f_s/2}$ and $\tau_{Rx, f_s/4}$.

2) *Estimation of Rx IQ Power Imbalance*: The Rx IQ power imbalance can be calculated by the power ratio between the Q and the I tributaries of the received signal, which can be defined as

$$g_{Rx,IQ}^2 = g_{Rx}^2 \frac{E[|s_{Rx,Q}(t + \tau_{Rx})|^2]}{E[|s_{Rx,I}(t)|^2]} = g_{Rx}^2 \frac{E[|s_{Rx,Q}(t)|^2]}{E[|s_{Rx,I}(t)|^2]} \quad (21)$$

Due to the independence between the $f_s/2$ and $f_s/4$ tones, we can extract Rx IQ power imbalance using only the $f_s/2$ tone or $f_s/4$ tone. The power ratio between the Q and I tributaries of $f_s/2$ tone can be calculated by

$$g_{Rx, f_s/2}^2 = g_{Rx}^2 \frac{E[|r_{f_s/2,Q}(t)|^2]}{E[|r_{f_s/2,I}(t)|^2]} \quad (22)$$

The power ratio between the Q and I tributaries of $f_s/4$ tone can be calculated by

$$g_{Rx, f_s/4}^2 = g_{Rx}^2 \frac{E[|r_{f_s/4,Q}(t)|^2]}{E[|r_{f_s/4,I}(t)|^2]} \quad (23)$$

The divisions of Eqs. (22) and (23) can be defined as

$$\frac{E[|r_{f_s/2,Q}(t)|^2]}{E[|r_{f_s/2,I}(t)|^2]} = \frac{E[|I_{f_s/2}(t)|^2 + |Q_{f_s/2}(t)|^2] + C_{f_s/2}}{E[|I_{f_s/2}(t)|^2 + |Q_{f_s/2}(t)|^2] - C_{f_s/2}} \quad (24)$$

and

$$\frac{E[|r_{f_s/4,Q}(t)|^2]}{E[|r_{f_s/4,I}(t)|^2]} = \frac{E[|I_{f_s/4}(t)|^2 + |Q_{f_s/4}(t)|^2] + C_{f_s/4}}{E[|I_{f_s/4}(t)|^2 + |Q_{f_s/4}(t)|^2] - C_{f_s/4}}, \quad (25)$$

respectively where

$$C_{f_s/2} = 2E[I_{f_s/2}(t)Q_{f_s/2}(t)\sin 2\phi_1(t)] \quad (26)$$

and

$$C_{f_s/4} = 2E[I_{f_s/4}(t + \tau_{Tx})Q_{f_s/4}(t + \tau_{Tx})\sin 2\phi_2(t)] \quad (27)$$

The existing frequency offset causes a varied $\phi_1(t)$ and $\phi_2(t)$ with a rotation of 2π . Therefore, $C_{f_s/2}$ and $C_{f_s/4}$ are equal

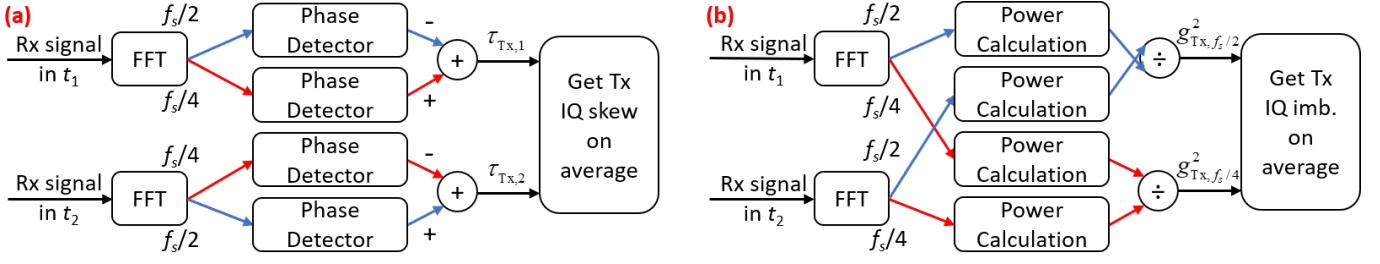


Fig. 5. Schematic diagram of far-end IQ-impairments estimation based on the specially designed TFITs including Tx IQ (a) skew and (b) power imbalance.

to zero. In theory, the $g_{\text{Rx}, f_s/2}^2$ and $g_{\text{Rx}, f_s/4}^2$ are both equal to the adding Rx IQ power imbalance g_{Rx}^2 .

Figure 4(b) shows the schematic diagram for Rx IQ power imbalance estimation by using the I and Q tributaries of the Rx TFITs. After FFT, two $f_s/2$ tones and two $f_s/4$ tones on the I and Q tributaries are extracted, respectively. According to Paswal's theorem, $g_{\text{Rx}, f_s/2}^2$ can be calculated by the power ratio between the two $f_s/2$ tones extracted from I and Q tributaries. Meanwhile, $g_{\text{Rx}, f_s/4}^2$ can be calculated by the power ratio between the extracted two $f_s/4$ tones from I and Q tributaries. It can improve the accuracy by filtering out the noise at the frequencies outside $f_s/2$ and $f_s/4$. Finally, the more accurate Rx IQ power imbalance $g_{\text{Rx}, \text{IQ}}^2$ can be obtained by averaging the $g_{\text{Rx}, f_s/2}^2$ and $g_{\text{Rx}, f_s/4}^2$.

D. Estimation of Tx IQ Impairments in PtMP Networks

After compensating for the Rx IQ impairments, the Rx TFITs suffer from the Tx IQ impairments, which can be expressed as Eqs. (12)-(14). $s_{\text{Rx}}(t)$ in the time slot t_i is denoted as $s_{\text{Rx}, t_i}(t)$ where $i = 1, 2$, which can be expressed as

$$s_{\text{Rx}, t_1}(t) = s_{\text{Rx}, f_s/2, t_1}(t) + j s_{\text{Rx}, f_s/4, t_1}(t) \quad (28)$$

and

$$s_{\text{Rx}, t_2}(t) = s_{\text{Rx}, f_s/4, t_2}(t) + j s_{\text{Rx}, f_s/2, t_2}(t), \quad (29)$$

respectively. In the time slot t_1 , the $s_{\text{Rx}, f_s/4, t_1}(t)$ suffers from the Tx IQ skew and power imbalance. In the time slot t_2 , the $s_{\text{Rx}, f_s/2, t_2}(t)$ suffers from the Tx IQ skew and power imbalance. Based on the model of IQ impairments, we propose TFITs-based schemes for accurately estimating the Tx IQ skew and power imbalance.

1) *Estimation of Tx IQ Skew*: In the time slot t_1 , $s_{\text{Rx}, f_s/2, t_1}(t)$ in the Eq. (13) suffers from the timing phase offset caused by the out-of-synchronization clock, while $s_{\text{Rx}, f_s/4, t_1}(t)$ in the Eq. (14) suffers from both the timing phase offset of the clock and Tx IQ skew τ_{Tx} . Therefore, the Tx IQ skew τ_{Tx} can be calculated by the difference in timing phase offset between $f_s/4$ and $f_s/2$ tones in the time slot t_1 . Similarly, the Tx IQ skew can be also calculated by the difference in timing phase offset between $f_s/2$ and $f_s/4$ tones in the time slot t_2 .

Figure 5(a) shows the schematic diagram of Tx IQ skew estimation based on the TFITs. By performing sampling and FFT on the Rx signal $s_{\text{Rx}, t_1}(t)$ in the time slots t_1 to $s_{\text{Rx}, t_1}(k)$ and $s_{\text{Rx}, t_2}(t)$ in the time slots t_2 to $s_{\text{Rx}, t_2}(k)$, the

timing phase offset of $f_s/2$ and $f_s/4$ tones are estimated by the Godard phase detector and the modified Godard phase detector, respectively. Thus, the Tx IQ skew can be estimated by subtracting the timing phase offset of the $f_s/2$ and $f_s/4$ tones in the time slot t_1 as

$$\begin{aligned} \tau_{\text{Tx}, t_1} &= \tau_{\text{Tx}} + \Delta\tau(f_s/4, f_s/2) \\ &= \frac{1}{\pi} \arg \left[\sum_{k=3N/8-n+1}^{3N/8+n} S_{\text{Rx}, t_1}(k) S_{\text{Rx}, t_1}^* \left(k + \frac{N}{4} \right) \right] \\ &\quad - \frac{1}{2\pi} \arg \left[\sum_{k=N/4-n+1}^{N/4+n} S_{\text{Rx}, t_1}(k) S_{\text{Rx}, t_1}^* \left(k + \frac{N}{2} \right) \right] \end{aligned} \quad (30)$$

where $\Delta\tau(f_s/4, f_s/2)$ denotes the additional timing offset caused by phase frequency response between the $f_s/2$ and $f_s/4$ tones. The Tx IQ skew can be also estimated by using the tones at $f_s/2$ and $f_s/4$ at time slot t_2 as

$$\begin{aligned} \tau_{\text{Tx}, t_2} &= \tau_{\text{Tx}} + \Delta\tau(f_s/2, f_s/4) \\ &= \frac{1}{2\pi} \arg \left[\sum_{k=N/4-n+1}^{N/4+n} S_{\text{Rx}, t_2}(k) S_{\text{Rx}, t_2}^* \left(k + \frac{N}{2} \right) \right] \\ &\quad - \frac{1}{\pi} \arg \left[\sum_{k=3N/8-n+1}^{3N/8+n} S_{\text{Rx}, t_2}(k) S_{\text{Rx}, t_2}^* \left(k + \frac{N}{4} \right) \right] \end{aligned} \quad (31)$$

where $\Delta\tau(f_s/2, f_s/4)$ denotes the additional timing offset caused by phase frequency response between $f_s/2$ and $f_s/4$ tones. Since the frequencies of tones are interleaved at the two time slots, $\Delta\tau(f_s/4, f_s/2)$ is equal to $-\Delta\tau(f_s/2, f_s/4)$. Therefore, the Tx IQ skew $\tau_{\text{Tx}, \text{IQ}}$ can be accurately acquired by averaging τ_{Tx, t_1} and τ_{Tx, t_2} at time slots t_1 and t_2 .

2) *Estimation of Tx IQ Power Imbalance*: The Tx IQ power imbalance can be calculated by the power ratio between two same-frequency tones at two time slots. The power ratio between two $f_s/2$ tones at the t_2 and t_1 time slots can be calculated by

$$g_{\text{Tx}, f_s/2}^2 = \frac{E(|s_{\text{Rx}, f_s/2, t_2}(t)|^2)}{E(|s_{\text{Rx}, f_s/2, t_1}(t)|^2)} = g_{\text{Tx}}^2 \frac{P_{f_s/2, t_2}}{P_{f_s/2, t_1}} \quad (32)$$

where $P_{f_s/2, t_1}$ and $P_{f_s/2, t_2}$ denote the average power of the $f_s/2$ tones without power imbalance in the time slots t_1 and

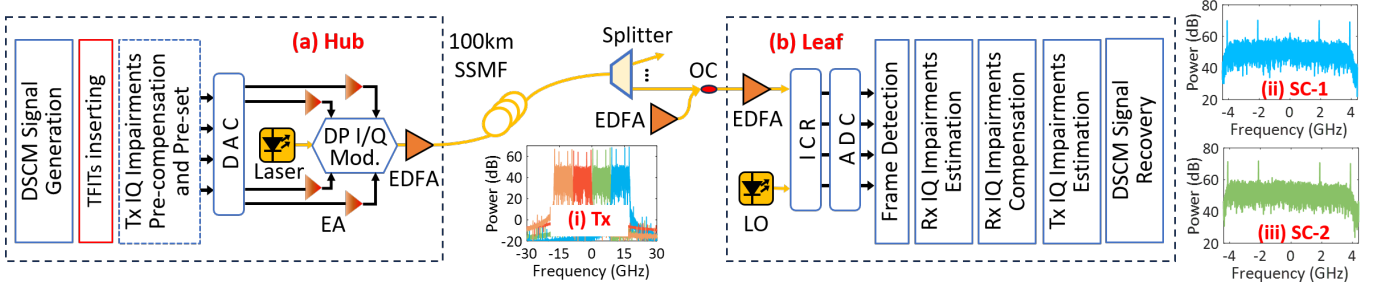


Fig. 6. The experimental setups of the coherent optical PtMP network to verify the feasibility of the TFITs-based far-end IQ-impairments estimation. Inset (i) is the electrical spectrum of the DSCM signal at the hub. Insets (ii) and (iii) are the electrical spectra of the received SC-1 and SC-2 at the leaf.

t_2 , respectively. Similarly, the power ratio between two $f_s/4$ tones at the t_1 and t_2 time slots can be calculated by

$$g_{Tx, f_s/4}^2 = \frac{E(|s_{Rx, f_s/4, t_1}(t)|^2)}{E(|s_{Rx, f_s/4, t_2}(t)|^2)} = g_{Tx}^2 \frac{P_{f_s/4, t_1}}{P_{f_s/4, t_2}} \quad (33)$$

where $P_{f_s/4, t_1}$ and $P_{f_s/4, t_2}$ denote the average power of the $f_s/4$ tones without power imbalance in the time slots t_1 and t_2 , respectively. The divisions in Eqs. (32) and (33) can be calculated by

$$\frac{P_{f_s/2, t_2}}{P_{f_s/2, t_1}} = \frac{E(|I_{f_s/2}(t + \tau_{Tx})|^2 + |Q_{f_s/2}(t + \tau_{Tx})|^2)}{E(|I_{f_s/2}(t)|^2 + |Q_{f_s/2}(t)|^2)} = 1 \quad (34)$$

and

$$\frac{P_{f_s/4, t_1}}{P_{f_s/4, t_2}} = \frac{E(|I_{f_s/4}(t + \tau_{Tx})|^2 + |Q_{f_s/4}(t + \tau_{Tx})|^2)}{E(|I_{f_s/4}(t)|^2 + |Q_{f_s/4}(t)|^2)} = 1, \quad (35)$$

respectively. Fig. 5(b) shows the estimation of Tx IQ power imbalance based on the TFITs. After the FFT, the average powers of $f_s/2$ and $f_s/4$ tones at the two time slots are separately calculated. It can improve the accuracy by filtering out the noise at the frequencies outside of $f_s/2$ and $f_s/4$. The Tx IQ power imbalance $g_{Tx, IQ}^2$ can be obtained by $g_{Tx, f_s/2}^2$ and $g_{Tx, f_s/4}^2$. Finally, the estimation accuracy of $g_{Tx, IQ}^2$ can be improved by averaging the $g_{Tx, f_s/2}^2$ and $g_{Tx, f_s/4}^2$.

III. EXPERIMENTAL SETUPS

Figure 6 shows the experimental setups of an 8Gbaud/SC \times 4SCs DSCM-based coherent PtMP optical network to verify the feasibility of the TFITs-based far-end IQ-impairments estimation. At the hub, the bit sequence was mapped to 16 quadrature amplitude modulation (16QAM) symbols. Then a root-raised cosine (RRC) pulse shaping filter with a roll-off factor of 0.1 was used for each subcarrier. After the frequency shift, the four subcarriers were multiplexed to generate a DSCM signal. The specially designed IQ TFITs were inserted before the DSCM signal for estimating the IQ impairments. A pre-compensation of Tx IQ impairments for the DSCM signal was implemented at the hub based on the far-end estimated IQ impairments at the leaf.

To verify the universality of the TFITs-based far-end IQ-impairments estimation, pre-set Tx IQ impairments were added to the digital DSCM signal. After adding pre-set Tx

IQ impairments, the digital signal was converted to the analog signal by a digital-to-analog converter (DAC) with a sampling rate of 90GSa/s. Inset (i) in Fig. 6 shows the electrical spectrum of the DSCM signal at the hub. An external cavity laser (ECL) operating at 1550.12nm with a less than 100kHz linewidth was used as the optical carrier. After being amplified by electrical amplifiers (EAs), the analog signal drove a dual-polarizations IQ modulator (DP I/Q Mod.) to generate the optical signal. The output optical power was approximately -14dBm. After being boosted by an Erbium-doped fiber amplifier (EDFA) to approximately 6 dBm, the optical signal was launched into a 100 km standard single-mode fiber (SSMF).

The optical signal is coupled with the optical white noise generated by EDFA by a 90:10 optical coupler (OC) to adjust the optical SNR (OSNR). At the leaf, the received optical signal was amplified by an EDFA to achieve an optical power of -10dBm. Then, the optical signal was detected by an integrated coherent receiver (ICR) to obtain the electrical signals. A tunable ECL with a linewidth less than 100 kHz was used as the LO, which has an output optical power of approximately 12dBm. The LO wavelength was tuned to match the central wavelength of the subcarrier for dropping the corresponding subband [32]. The electrical signals were digitized by a 90GSa/s analog-to-digital converter (ADC) and then recovered by the Rx digital signal processing (DSP).

Insets (ii) and (iii) in Fig. 6 are the received spectra of the SC-1 and SC-2 at the leaf, respectively. Without loss of generality, SC-1 and SC-2 were used to estimate the IQ impairments. After frame detection, Rx IQ skew and power imbalance were estimated based on the specially designed TFITs and proposed algorithms. The Rx IQ power imbalance can be compensated by multiplying an estimated coefficient $1/g_{Rx, IQ}$ in Eq. (21) on the Q tributary. Meanwhile, the Rx IQ skew can be effectively compensated by interpolation based on $\tau_{Rx, IQ}$. After compensating Rx IQ impairments, the Tx IQ skew $\tau_{Tx, IQ}$ and power imbalance $g_{Tx, IQ}$ were estimated by the specially designed TFITs and proposed algorithms and then transmitted to the hub using the uplink. After the IQ impairments estimation, the DSCM signal was recovered by DSP as demonstrated in Refs. [33]–[35].

IV. EXPERIMENTAL RESULTS AND DISCUSSIONS

Firstly, the TFITs-based IQ-impairments estimation is evaluated when only IQ skew or power imbalance exists. The OSNR

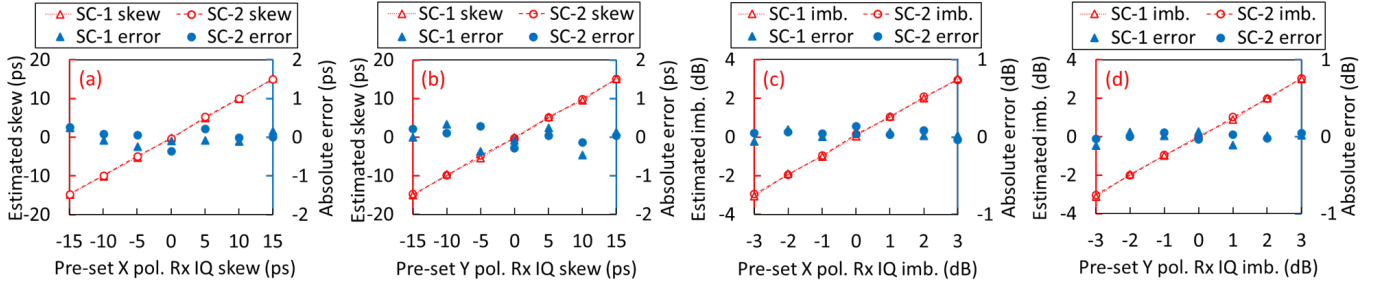


Fig. 7. Estimated Rx IQ impairments versus pre-set Rx IQ impairments and the absolute error between the estimated Rx IQ impairments and pre-set Rx IQ impairments. (a) X polarization Rx IQ skew, (b) Y polarization Rx IQ skew, (c) X polarization Rx IQ power imbalance, and (d) Y polarization Rx IQ imbalance. The Pol. denotes Polarization. The Imb. denotes Imbalance.

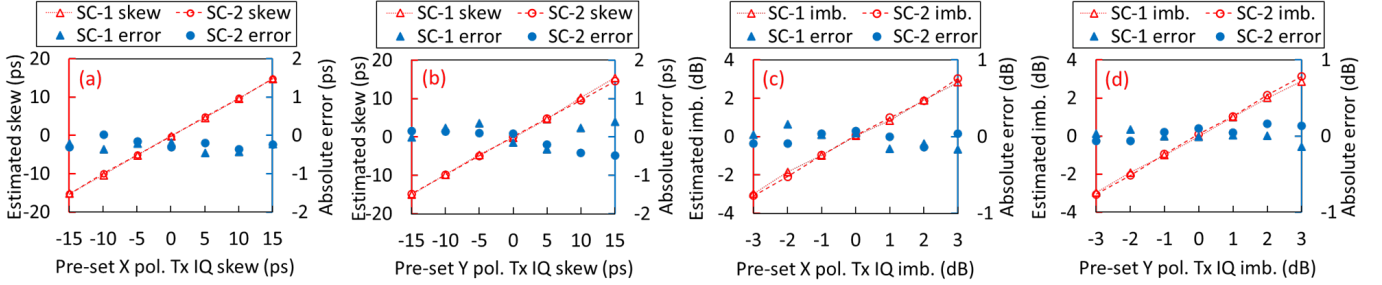


Fig. 8. Estimated Tx IQ impairments versus pre-set Tx IQ impairments and the absolute error between the estimated Tx IQ impairments and pre-set Tx IQ impairments. (a) X polarization Tx IQ skew, (b) Y polarization Tx IQ skew, (c) X polarization Tx IQ imbalance, and (d) Y polarization Tx IQ imbalance.

was set to approximately 17dB for verifying the robustness of TFITs-based IQ-impairments estimation under large enough noise. Figs. 7(a) and (b) show the estimated Rx IQ skews versus pre-set Rx IQ skews and the absolute errors between the estimated Rx IQ skews and pre-set Rx IQ skews for X and Y polarizations, respectively. When the Rx IQ skews were set to the values from -15ps to 15ps (i.e. 24% of the symbol duration) on X and Y polarizations, the TFITs-based Rx IQ skew estimation can achieve the absolute error within $\pm 0.5\text{ps}$. Figs. 7(c) and (d) show the estimated Rx IQ power imbalances versus pre-set Rx IQ power imbalances and the absolute errors between the estimated Rx IQ power imbalances and pre-set Rx IQ power imbalances for X and Y polarizations, respectively. When the Rx IQ imbalances were set to the values from -3dB to 3dB , the TFITs-based Rx IQ power imbalance estimation can achieve an absolute error within $\pm 0.2\text{dB}$.

Figures 8(a) and (b) show the estimated Tx IQ skews versus pre-set Tx IQ skews and the absolute errors between the estimated Tx IQ skews and pre-set Tx IQ skews for the X and Y polarizations, respectively. When only the Tx IQ skews were set to the values from -15ps to 15ps on X and Y polarizations, the TFITs-based far-end Tx IQ-skew estimation can achieve the absolute error within $\pm 0.5\text{ps}$. Figs. 8(c) and (d) depict the estimated Tx IQ power imbalances versus pre-set Tx IQ power imbalances and the absolute errors between the estimated Tx IQ power imbalances and pre-set Tx IQ power imbalances for the X and Y polarizations, respectively. When the Tx IQ power imbalances were set to the values from -3dB to 3dB , the TFITs-based far-end Tx IQ-power-imbalance estimation can achieve an absolute error within $\pm 0.2\text{dB}$.

The TFITs-based IQ-impairments estimation is also eval-

uated when several IQ impairments coexist. Fig. 9(a) shows the estimated Rx IQ skew versus pre-set Rx IQ skew, and the absolute error between the estimated Rx IQ skew and pre-set Rx IQ skew when 5ps Tx IQ skew, 1dB Tx IQ power imbalance, and -1dB Rx IQ power imbalance coexist. The Rx IQ skew from -15ps to 15ps can be estimated with the absolute error within $\pm 0.5\text{ps}$ by using TFITs-based Rx IQ-skew estimation. Fig. 9(b) shows the estimated Rx IQ power imbalance versus pre-set Rx IQ power imbalance, and the absolute error between estimated Rx IQ power imbalance and pre-set Rx IQ power imbalance when 5ps Tx IQ skew, 1dB Tx IQ power imbalance, and -5ps Rx IQ skew coexist. The Rx IQ power imbalance from -3dB to 3dB can be estimated with the absolute error within $\pm 0.2\text{dB}$ by using TFITs-based Rx IQ-power-imbalance estimation.

Figure 9(c) shows the estimated Tx IQ skew versus pre-set Tx IQ skew and the absolute error between the estimated Tx IQ skew and pre-set Tx IQ skew when 1dB Tx IQ power imbalance, -5ps Rx IQ skew, and -1dB Rx IQ power imbalance coexist. The Tx IQ skew from -15ps to 15ps can be estimated with the absolute error within $\pm 0.5\text{ps}$ by TFITs-based far-end Tx IQ-skew estimation. Fig. 9(d) shows the estimated Tx IQ power imbalance versus pre-set IQ power imbalance and the absolute error between estimated IQ power imbalance and pre-set IQ power imbalance when 5ps Tx IQ skew, -5ps Rx IQ skew, and -1dB Rx IQ power imbalance coexist. The Tx IQ power imbalance from -3dB to 3dB can be estimated with the absolute error within $\pm 0.2\text{dB}$ by TFITs-based far-end Tx IQ-power-imbalance estimation. In conclusion, TFITs-based IQ-impairments estimation can accurately estimate Rx and Tx IQ impairments at the far-end leaf.

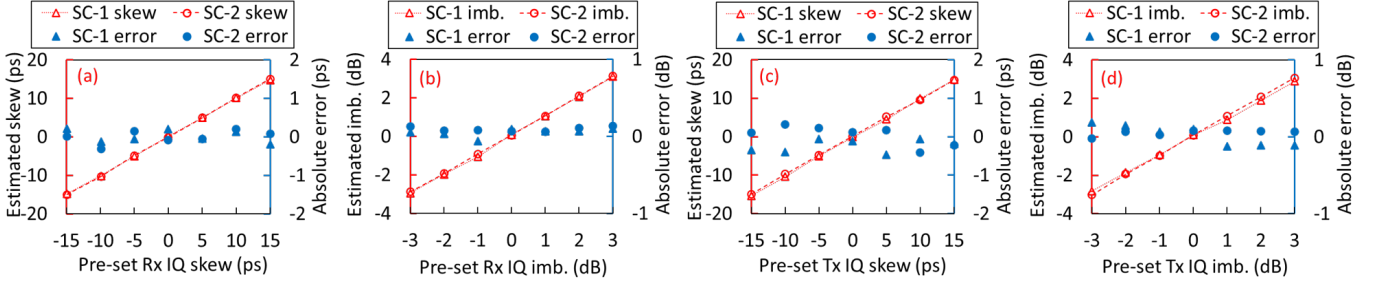


Fig. 9. Estimated IQ impairments versus pre-set IQ impairments and the absolute error between the estimated IQ impairments and pre-set IQ impairments under (a) 5ps Tx IQ skew, 1dB Tx IQ power imbalance, and -1 dB Rx IQ power imbalance, (b) 5ps Tx IQ skew, 1dB Tx IQ power imbalance, and -5 ps Rx IQ skew, (c) 1dB Tx IQ power imbalance, -5 ps Rx IQ skew, and -1 dB Rx IQ power imbalance, and (d) 5ps Tx IQ skew, -5 ps Rx IQ skew, and -1 dB Rx IQ power imbalance, respectively.

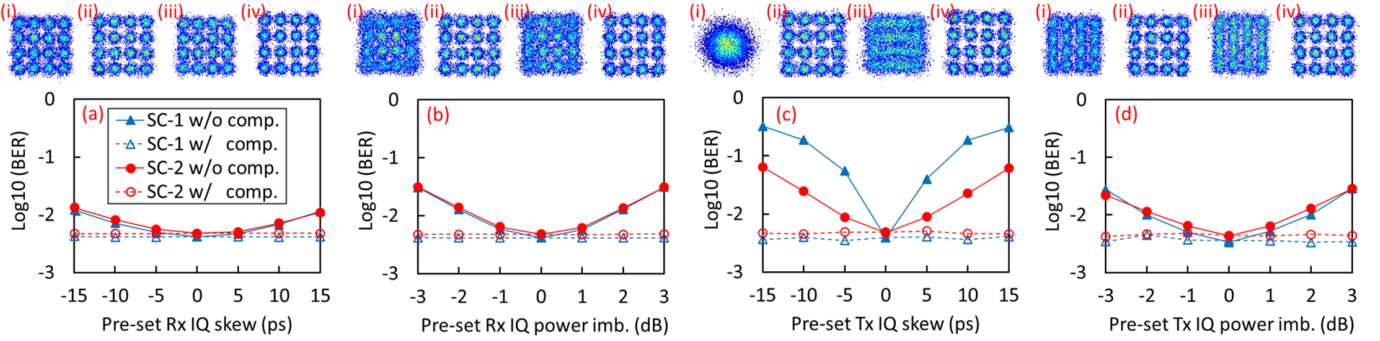


Fig. 10. BER performance at SC-1 and SC-2 versus (a) Rx IQ skew, (b) Rx IQ power imbalance, (c) Tx IQ skew, (d) IQ power imbalance without (w/o) and with (w/) compensation (comp.). Insets are the constellation diagrams of (i) SC-1 without compensation, (ii) SC-1 with compensation, (iii) SC-2 without compensation, and (iv) SC-2 with compensation, respectively.

In 8Gbaud/SC \times 4SCs DSCM-based coherent PtMP optical network, the bit-error ratios (BERs) of SC-1 and SC-2 are used to evaluate the effect of IQ-impairments estimation and compensation. The OSNR was set to approximately 22dB to ensure the BER can achieve 0.0038. As Figs. 10(a) and (b) show, the BERs of the SC-1 and SC-2 increase with the increase of Rx IQ skew or power imbalance. Insets of Figs. 10(a) and (b) depict the constellation diagrams under 15ps Rx IQ skew or 3dB Rx IQ power imbalance of (i) SC-1 without compensation, (ii) SC-1 with compensation, (iii) SC-2 without compensation, and (iv) SC-2 with compensation, respectively. After compensation for Rx IQ impairments, the BER penalties caused by Rx IQ skews or power imbalances are almost eliminated, and the constellations are clearer. Significantly, the impacts of the Rx IQ impairments on the BERs of the SC-1 and SC-2 are similar because the two subcarriers are detected as the baseband signals at the leaf.

Figures 10(c) and (d) depict the BERs of the SC-1 and SC-2 under the Tx IQ skews and Tx IQ power imbalances, respectively. Insets of Figs. 10(c) and (d) show the constellation diagrams under 15ps Tx IQ skew or 3dB Tx IQ power imbalance of (i) SC-1 without compensation, (ii) SC-1 with compensation, (iii) SC-2 without compensation, and (iv) SC-2 with compensation, respectively. Since the image crosstalk caused by Tx IQ skew increases with the frequency increase, higher-frequency SC-1 suffers from more distortions than lower-frequency SC-2. Thus, the BER performance of SC-1 is more sensitive to Tx IQ skew than that of SC-

2. Since the image crosstalk caused by the Tx IQ power imbalance is the same on all the frequencies, the higher-frequency SC-1 suffers from almost the same distortions as the lower-frequency SC-2, leading to the same trend of BER performance degradation. After compensation for Tx IQ impairments, the BER penalty on the two subcarriers can be almost eliminated, and the constellations become much clearer. In conclusion, the proposed IQ-impairments estimation and compensation can effectively improve the BER performance for the DSCM-based coherent PtMP optical networks.

V. CONCLUSION

In this paper, the TFITs are designed to implement the far-end IQ-impairments estimation for DSCM-based coherent PtMP optical networks. The TFITs-based far-end IQ-impairments estimation does not require the signals on two symmetrical subcarriers, which can estimate Tx IQ skew and power imbalance of hub at an individual leaf. The 8Gbaud/SC \times 4SCs DSCM-based coherent PtMP optical network is experimentally demonstrated to verify the feasibility of TFITs-based IQ-impairments estimation. The experimental results depict that TFITs-based IQ-impairments estimation can achieve absolute errors in IQ skew and power imbalance within ± 0.5 ps and ± 0.2 dB, respectively. After compensation for the IQ impairments, the BER performance can be significantly improved, especially the high-frequency subcarriers. In conclusion, TFITs-based IQ-impairments estimation has great potential for DSCM-based coherent PtMP optical networks.

REFERENCES

- [1] L. A. Campos, Z. Jia, H. Zhang, and M. Xu, "Coherent optics for access from P2P to P2MP," *Journal of Optical Communications and Networking*, vol. 15, no. 3, pp. A114–A123, 2023.
- [2] Y. Zhang, Q. Lv, R. Li, X. Tian, and Z. Zhu, "Planning of Survivable Wavelength-Switched Optical Networks based on P2MP Transceivers," *IEEE Transactions on Network and Service Management*, vol. 20, no. 3, pp. 2331–2342, 2023.
- [3] C. Castro, A. Napoli, M. Porrega, J. Bäck, A. Rashidinejad, M. Quagliotti, E. Riccardi, D. Hillerkuss, A. Yekani, F. Masoud, *et al.*, "Scalable filterless coherent point-to-multipoint metro network architecture," *Journal of Optical Communications and Networking*, vol. 15, no. 5, pp. B53–B66, 2023.
- [4] D. Welch, A. Napoli, J. Bäck, W. Sande, J. Pedro, F. Masoud, C. Fludger, T. Duthel, H. Sun, S. J. Hand, *et al.*, "Point-to-multipoint optical networks using coherent digital subcarriers," *Journal of Lightwave Technology*, vol. 39, no. 16, pp. 5232–5247, 2021.
- [5] D. Welch, A. Napoli, J. Bäck, S. Buggaveeti, C. Castro, A. Chase, X. Chen, V. Dominic, T. Duthel, T. A. Eriksson, *et al.*, "Digital subcarrier multiplexing: Enabling software-configurable optical networks," *Journal of Lightwave Technology*, vol. 41, no. 4, pp. 1175–1191, 2023.
- [6] A. Rashidinejad, A. Yekani, T. A. Eriksson, A. Napoli, R. Maher, A. Kakkar, V. Dominic, T. Duthel, M. Missey, P. Samra, *et al.*, "Real-Time Point-to-Multipoint for Coherent Optical Broadcast and Aggregation-Enabled by Digital Subcarrier Multiplexing," in *Optical Fiber Communication Conference*, pp. W3H–1, Optica Publishing Group, 2023.
- [7] P. Pavon-Marino, N. Skorin-Kapov, M. Bueno-Delgado, J. Bäck, and A. Napoli, "On the benefits of point-to-multipoint coherent optics for multilayer capacity planning in ring networks with varying traffic profiles," *Journal of Optical Communications and Networking*, vol. 14, no. 5, pp. B30–B44, 2022.
- [8] P. Pavon-Marino, N. Skorin-Kapov, and A. Napoli, "Tree-determination, routing, and spectrum assignment using point-to-multipoint coherent optics," *Journal of Optical Communications and Networking*, vol. 15, no. 7, pp. C29–C40, 2023.
- [9] Z. Xing, K. Zhang, X. Chen, Q. Feng, K. Zheng, Y. Zhao, Z. Dong, J. Zhou, T. Gui, Z. Ye, *et al.*, "First Real-time Demonstration of 200G TFDMA Coherent PON using Ultra-simple ONUs," in *Optical Fiber Communication Conference*, pp. Th4C–4, Optica Publishing Group, 2023.
- [10] T. Zhang, C. Sanchez, S. Sygletos, and A. Ellis, "800G/λ transponder based on joint subband processing and subcarrier multiplexing," in *45th European Conference on Optical Communication (ECOC 2019)*, pp. 1–4, IET, 2019.
- [11] T. Duthel, C. R. Fludger, B. Liu, A. Napoli, A. Rashidinejad, S. Ranzini, S. Erkilinc, A. Kakkar, A. Mathur, V. Dominic, *et al.*, "DSP Design for Point-to-Multipoint Transmission," in *Optical Fiber Communication Conference*, pp. W1E–1, Optica Publishing Group, 2023.
- [12] W. Tong, J. Zhang, M. Zhu, X. Liu, Y. Wei, B. Hua, Z. Xin, M. Lei, Y. Cai, Y. Zou, *et al.*, "Experimental Comparison of Single-Carrier and Digital Subcarrier Multiplexing Transmissions in a W-Band 200 Gb/s Fiber-wireless System Considering Transmitter IQ Imbalance and Skew Mitigation," *IEEE Photonics Journal*, vol. 15, no. 4, p. 5501308, 2023.
- [13] G. Bosco, S. M. Bilal, A. Nespola, P. Poggiolini, and F. Forghieri, "Impact of the transmitter IQ-skew in multi-subcarrier coherent optical systems," in *Optical Fiber Communication Conference*, pp. W4A–5, Optica Publishing Group, 2016.
- [14] L. Fan, Y. Yang, S. Gong, C. Cheng, Q. Xiang, Q. Zhang, and Y. Yao, "Hardware-efficient and robust DSP scheme for coherent DSCM system in presence of transmitter IQ impairments," *Journal of Lightwave Technology*, vol. 41, no. 19, pp. 6187–6198, Oct. 2023.
- [15] T. Duthel, C. R. Fludger, B. Liu, S. Ranzini, A. Napoli, N. Sölch, S. M. Bilal, S. B. Amado, S. Alreesh, J. Sime, *et al.*, "DSP Design for Coherent Optical Point-to-Multipoint Transmission," *Journal of Lightwave Technology*, 2023.
- [16] Y. Fan, X. Su, H. Chen, J. Liang, Z. Tao, H. Nakashima, and T. Hoshida, "Experimental verification of IQ imbalance monitor for high-order modulated transceivers," in *2018 European Conference on Optical Communication (ECOC)*, pp. 1–3, IEEE, 2018.
- [17] J. Liang, Y. Fan, Z. Tao, X. Su, and H. Nakashima, "Transceiver imbalances compensation and monitoring by receiver DSP," *Journal of Lightwave Technology*, vol. 39, no. 17, pp. 5397–5404, 2019.
- [18] Y. Fan, Y. Jiang, J. Liang, Z. Tao, H. Nakashima, and T. Hoshida, "Transceiver IQ imperfection monitor by digital signal processing in coherent receiver," in *2019 24th OptoElectronics and Communications Conference (OECC) and 2019 International Conference on Photonics in Switching and Computing (PSC)*, pp. 1–3, IEEE, 2019.
- [19] Z. Zhai, M. Fu, L. Liu, H. Jiang, H. Ren, L. Yi, W. Hu, and Q. Zhuge, "Transmitter IQ mismatch compensation and monitoring for digital subcarrier-multiplexing systems," in *Asia Communications and Photonics Conference*, pp. M4A–319, Optica Publishing Group, 2020.
- [20] W. C. Ng, H. Qin, Y. Wang, X. Tang, and C. Li, "Far-end Receiver DSP-based Transmitter Imbalance for Digital Subcarrier Multiplexing Systems," in *Signal Processing in Photonic Communications*, pp. SpTh11–7, Optica Publishing Group, 2022.
- [21] L. Dai, D. Li, C. Huang, H. Li, Y. Yang, H. Song, M. Cheng, Q. Yang, M. Tang, D. Liu, *et al.*, "Hardware demonstration of simultaneously precise Tx and Rx skew calibration for coherent optical transceiver," *Journal of Lightwave Technology*, vol. 40, no. 4, pp. 1043–1054, 2022.
- [22] L. Dai, C. Huang, H. Li, M. Cheng, Q. Yang, M. Tang, D. Liu, and L. Deng, "Simultaneously precise frequency response and IQ skew calibration in a self-homodyne coherent optical transmission system," *Optics Express*, vol. 30, no. 12, pp. 20894–20908, 2022.
- [23] H. Chen, X. Su, Z. Tao, T. Oyama, H. Nakashima, T. Hoshida, and K. Kato, "An accurate and robust in-phase/quadrature skew measurement for coherent optical transmitter by image spectrum analyzing," in *2017 European Conference on Optical Communication (ECOC)*, pp. 1–3, IEEE, 2017.
- [24] C. Zhu, N. Kaneda, and J. Lee, "Reception of Burst Mode High-Order QAM Signals with Pilot-Aided Digital Signal Processing," in *Optical Fiber Communication Conference*, pp. M1C–5, Optica Publishing Group, 2018.
- [25] J. Zhang, Z. Jia, M. Xu, H. Zhang, and L. A. Campos, "Efficient preamble design and digital signal processing in upstream burst-mode detection of 100G TDM coherent-PON," *Journal of Optical Communications and Networking*, vol. 13, no. 2, pp. A135–A143, 2021.
- [26] X. Liu and F. Buchali, "Intra-symbol frequency-domain averaging based channel estimation for coherent optical OFDM," *Optics Express*, vol. 16, no. 26, pp. 21944–21957, 2008.
- [27] Q. Zhang, Y. Yang, C. Gu, Y. Yao, A. P. T. Lau, and C. Lu, "Multi-dimensional, wide-range, and modulation-format-transparent transceiver imbalance monitoring," *Journal of Lightwave Technology*, vol. 39, no. 7, pp. 2033–2045, 2020.
- [28] W. Chung, "Transmitter IQ mismatch compensation in coherent optical OFDM systems using pilot signals," *Optics Express*, vol. 18, no. 20, pp. 21308–21314, 2010.
- [29] X. Wang, F. Li, M. Yin, Z. Luo, S. Qin, W. Wang, Y. Cai, and Z. Li, "Correlation-based transceiver in-phase/quadrature skew in-field calibration in dual-polarization coherent optical transmission system," *Optics Express*, vol. 30, no. 13, pp. 22712–22729, 2022.
- [30] D. Godard, "Passband timing recovery in an all-digital modem receiver," *IEEE Transactions on Communications*, vol. 26, no. 5, pp. 517–523, 1978.
- [31] K.-T. Wu and H. Sun, "Frequency-domain clock phase detector for Nyquist WDM systems," in *Optical Fiber Communication Conference*, pp. Th3E–2, Optica Publishing Group, 2014.
- [32] B. Zhang, C. Malouin, and T. J. Schmidt, "Towards full band colorless reception with coherent balanced receivers," *Optics Express*, vol. 20, no. 9, pp. 10339–10352, 2012.
- [33] H. Wang, J. Zhou, Z. Xing, Q. Feng, K. Zhang, K. Zheng, X. Chen, T. Gui, L. Li, J. Zeng, *et al.*, "Fast-Convergence Digital Signal Processing for Coherent PON using Digital SCM," *Journal of Lightwave Technology*, vol. 41, no. 14, pp. 4635–4643, 2023.
- [34] J. Zhou, Z. Xing, H. Wang, K. Zhang, X. Chen, Q. Feng, K. Zheng, Y. Zhao, Z. Dong, T. Gui, Z. Ye, and L. Li, "Flexible Coherent Optical Access: Architectures, Algorithms, and Demonstrations," *Journal of Lightwave Technology*, 2024.
- [35] H. Wang, J. Zhou, J. Yang, J. Zeng, W. Liu, C. Yu, F. Li, and Z. Li, "Non-integer-oversampling digital signal processing for coherent passive optical networks," *Journal of Optical Communications and Networking*, vol. 16, no. 1, pp. 4–11, 2024.